

Moving and jumping spot in a two dimensional reaction-diffusion model

Shuangquan Xie[†] and Theodore Kolokolnikov[†]

[†]*Department of Mathematics and Statistics, Dalhousie University, Halifax, Canada*

We consider a single spot solution for the Schnakenburg Model in a two-dimensional unit disk in the singularly perturbed limit of a small diffusivity ratio. For large values of the reaction-time constant, this spot can undergo two different types of instabilities, both due to a Hopf bifurcation. The first type induces oscillatory instability in the height of the spot. The second type induces a periodic motion of the spot center. We use formal asymptotics to investigate when these instabilities are triggered, and which one dominates. In the parameter regime where spot motion occurs, we construct a periodic solution consisting of a rotating spot, and compute its radius of rotation and angular velocity. Detailed numerical simulations are performed to validate the asymptotic theory, including rotating spots. More complex, non-circular spot trajectories are also explored numerically.

1. INTRODUCTION

The Schnakenburg model, introduced in [1], is a particular case of the activator-substrate system. It was originally formulated as a simplified model of a trimolecular autocatalytic reaction with diffusion. It is also a limiting case of both the Gray-Scott model as well as the Klausmeyer model of vegetation pattern formation on a flat ground when the water evaporation is limited [2]. Some applications of Schnakenburg model to biology include pattern formations in embryogenesis and skin patterns [3, 4]. However arguably its biggest value is that it serves as a simple prototype model for studying pattern formation in reaction-diffusion systems: it is among the simplest class of models which generate stable inhomogeneous patterns. As such, the Schnakenburg and related models such as Gray-Scott, the Brusselator, and the Gierer-Meinhardt model, have been extensively studied (especially in one, but also and two and higher dimensions), and phenomena such as spike formation, stability, self-replication, oscillations and motion has been analysed in detail. A very incomplete list of references includes [5–18].

In [7–9] the authors have found that a single spike in a one-dimensional Gray-Scott model can undergo destabilizing oscillations in *either* its height or position. The height oscillations happen on a much faster timescale when compared to the position oscillations. Which instability is triggered first depends on the value of the feed-rate A representing the amount of the substrate chemical that is being pumped into the system. Typically, height oscillations were triggered at lower feed rates than the position oscillations. Periodic spike motion in one dimensional GS model was further investigated in [17].

In one-dimensional domain, there has been much work over the past decade in analyzing the stability, dynamics, and self-replication of spike patterns for the Schakenberg model and related models with similar structure. The stability problem for equilibrium spike patterns in infinite domain has been studied in [14] and [11] following earlier work on Gierer-Meinhardt model [19]. In [20], the authors studied Hopf bifurcations and oscillatory instabilities of spike solutions of Gierer-Meinhardt model for various ranges of the reaction-time constant. For a recent summary on pattern formation in GM model, see [21] and references therein. A detailed study of self-replication, overcrowding instability, and spike height and position oscillations for the Gray-Scott model is conducted in [6–9, 17, 22]. Self-replication in slowly growing domains was also studied in [23] and [24].

In two dimensions, Muratov and Osipov [10] were among the first to study the Gray-Scott model, including self-replication thresholds. Wei and Winter [12] reviewed analytical methods for a rigorous study of the existence and stability of stationary, multiple spots for reaction-diffusion systems and considered two classes of reaction-diffusion systems: activator-inhibitor systems (such as the Gierer-Meinhardt system) and activator-substrate systems (such as the Gray-Scott system or the Schnakenburg model). In [13], spot replication for the Schnakenburg model was studied. In [16], the authors studied multi-spot patterns including competition, spot motion, and self-replication, for the related Gray-Scott model.

The purpose of this work is two-fold. First, we extend the results in [7–9] on thresholds for oscillatory instabilities for both height and spike position (and particularly periodically moving spikes) from one dimension to a two-dimensional setting. Second, we investigate the spot trajectory (i.e. the path traced by the spot center) and the kind of complex two-dimensional motion that can result.

We will use the following scaling of the Schakenberg model,

$$v_t = \varepsilon^2 \Delta v - v + v^2 u, \quad \tau u_t = \Delta u + A - \frac{v^2 u}{\varepsilon^2} \quad \text{inside } \Omega \subset \mathbb{R}^2; \quad \partial_n v = \partial_n u = 0 \quad \text{on } \partial\Omega. \quad (1.1)$$

Throughout this paper, we assume Ω to be a unit disk,

$$\Omega \text{ is a unit disk; } \Omega = \{x \in \mathbb{R}^2 : |x| < 1\}, \quad (1.2)$$

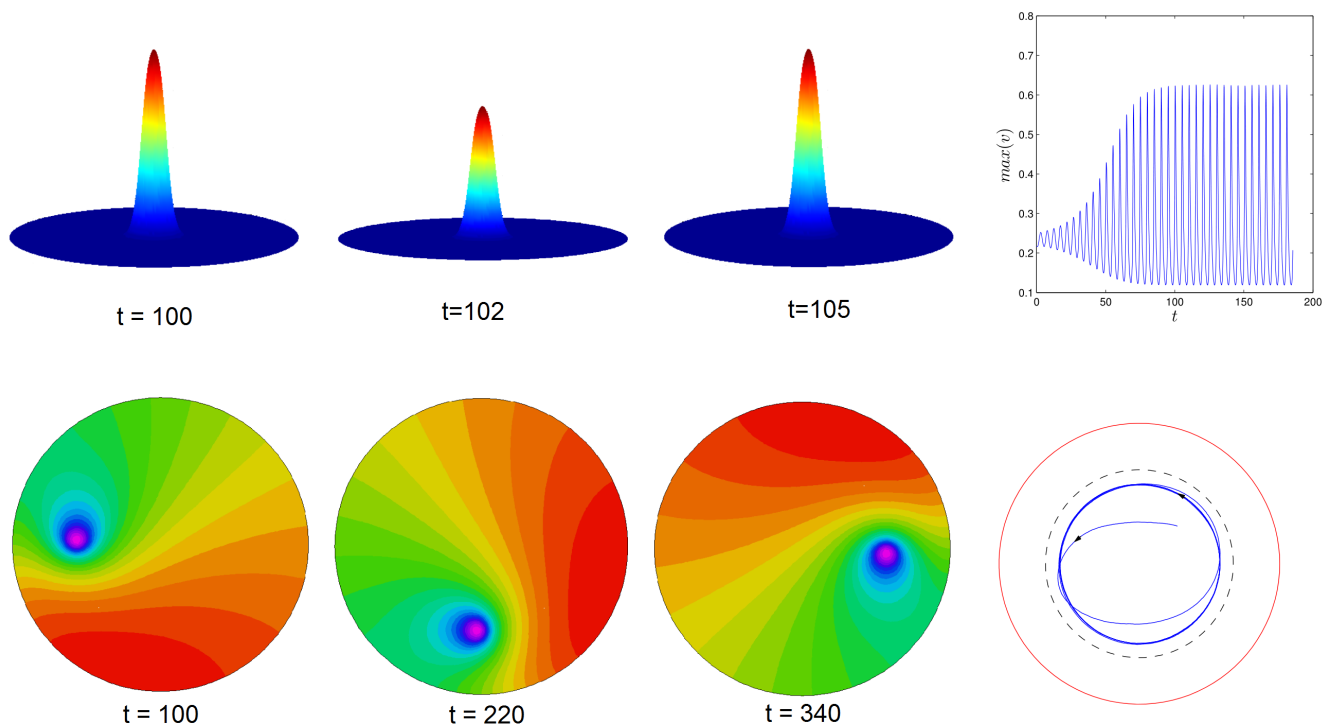


FIG. 1. Two types of dynamics of a single spike solution of the Schnakenberg model. Top row: height oscillations on $O(1)$ timescale. Three snapshots of $v(x, t)$ are shown at times as indicated. Parameters are $\varepsilon = 0.03, A = 1, \tau = 0.07$. Top right shows the height of the spike as a function of time. The spike remains at the center of the disk. Bottom row: periodic motion of the spot on a slow timescale. Three snapshots of $u(x, t)$ are shown. Bottom right shows the trajectory of the spot center. Parameters are $\varepsilon = 0.02, A = 8, \tau = 0.15/\varepsilon^2$. Dashed line shows the asymptotic prediction for the spot trajectory (Proposition 6.1)

although some of our results can be extended to more general domains.

Here, $\varepsilon \ll 1$, $A > 0$ and $\tau > 0$, represent diffusivity, the feed-rate and the reaction-time constant respectively. The equations model the following process: the fast-diffusing substrate u is consumed by a slowly diffusing activator v , which decays in time. The substrate is being pumped into the system at a constant rate, represented by parameter A . The reaction kinetics for u and v occur at different scales (depending on the choice of τ). Of particular interest to us will be the regime where τ is very large, so that u reacts much slower than v . As we will show, the oscillatory instabilities (both for spike height and positions) are triggered when τ is very large.

In this paper we consider the effect of increasing the parameter τ on a single spot at the center of the unit disk. The associated linearized eigenvalue problem has eigenfunctions of the form $\phi(r)e^{im\theta}$ in the polar coordinates. Due to underlying translational invariance, the eigenvalues corresponding to mode $m = \pm 1$ are asymptotically small as $\varepsilon \rightarrow 0$ and their instability induces a slow (possibly periodic) motion of the spot. We refer to these eigenvalues as *small eigenvalues*. All other eigenvalues are referred to as *large eigenvalues*. The mode $m = 0$ corresponds to purely radial perturbations and its instability can induce spike oscillation or collapse, whereas the instability with respect to mode $m = 2$ eigenvalues triggers self-replication [10, 13, 16, 25]. Here, we only concentrate on modes $m = 0, 1$ since τ does not appear to trigger instability of the higher modes.

Two different types of instabilities can be triggered when τ is sufficiently increased as illustrated in Figure 1: either large or small eigenvalues can undergo a Hopf bifurcation. The former instability triggers height oscillations, whereas the latter triggers slow translational instabilities in spike position, inducing (typically periodic) spike motion. Which one is triggered *first* depends on values of ε and A .

Our main task is to classify precisely for which parameters A and ε does the spike motion (as opposed to height oscillations) occur when τ is increased sufficiently? In §5 (Proposition 5.1) we give a concise characterisation in terms of the following threshold. Let

$$A_c \sim \frac{6.283}{\sqrt{\log \left\{ \left(\log \frac{1}{\varepsilon} \right) 1.010 - 0.1433 \right\}}}. \quad (1.3)$$

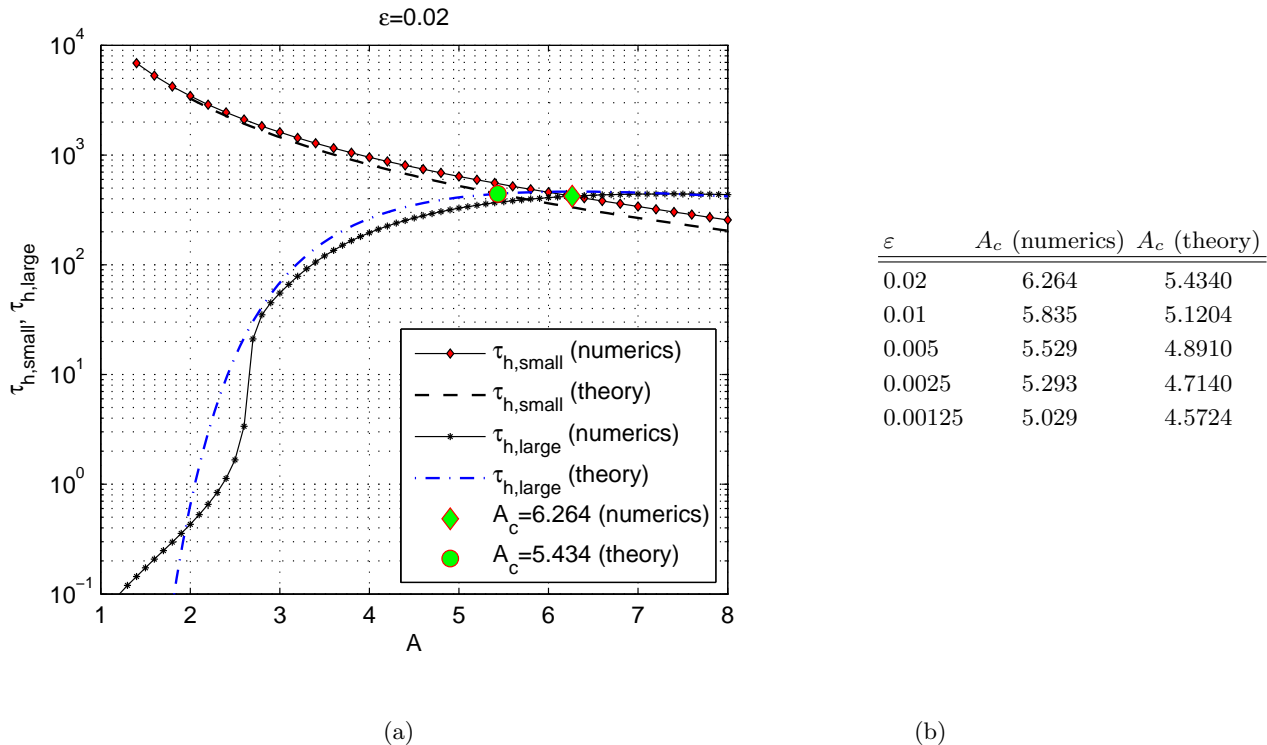


FIG. 2. (a) Hopf bifurcations values for height and position oscillations ($\tau_{h,large}$ and $\tau_{h,small}$, respectively), as a function of A , and with $\varepsilon = 0.02$. Theoretical predictions given by Propositions 3.1 and 4.1 are also shown. The intersection of $\tau_{h,large}$ and $\tau_{h,small}$ is denoted by A_c . (b) Comparison between the asymptotic value of A_c given by (1.3) and the numerically computed value for several small ε .

In the limit $\varepsilon \rightarrow 0$, for values of A bigger than A_c , spike motion is observed as τ is sufficiently increased, whereas when $A < A_c$, increasing τ triggers height oscillations. This threshold follows from computing the thresholds $\tau_{h,large}$ and $\tau_{h,small}$, corresponding to the Hopf bifurcation points for small and large eigenvalues, respectively. This is done in §3, and §4 to obtain

$$\tau_{h,large} \sim \frac{19.929}{A^2 \varepsilon^2} \exp\left(\frac{-39.474}{A^2}\right); \quad \tau_{h,small} \sim \frac{1}{\varepsilon^2 A^2} \frac{19.737}{\log \frac{1}{\varepsilon} - 0.1419} \quad (1.4)$$

in the critical regime $O\left(\frac{1}{\log 1/\varepsilon}\right) \ll A^2 \ll O(1)$. In fact the threshold (1.3) is obtained from (1.4) by simply setting $\tau_{h,large} = \tau_{h,small}$.

The threshold (1.3) has a striking log log scaling. Despite such a slow convergence rate, remarkably it agrees relatively well with numerical experiments even when $\varepsilon = 0.01$ (see Figure 2).

In §6 we analyse what happens beyond the Hopf bifurcation for small eigenvalues, in the regime $\tau_{h,small} < \tau < \tau_{h,large}$. In this regime, the spot starts to move and there exists time-dependent solutions in a form of a rotating spot. We compute the radius and speed of the rotation in Proposition 6.1. By computing the radius of rotation r_0 as a function of τ , we find that $r_0 \rightarrow 0$ as $\tau \rightarrow \tau_{h,small}$ from above. In other words, the rotating spot solution bifurcates from a stationary spot as a result of a Hopf bifurcation. This is illustrated in Figure 4. We conclude with numerical experiments demonstrating even more complex spike motion (see Figure 5).

2. EQUILIBRIUM SOLUTION

We start by reviewing the construction of the equilibrium solution to (1.1) using the method of matched asymptotic expansions as was previously done in [13]. At the equilibrium, the steady state satisfies

$$0 = \varepsilon^2 \Delta v - v + wv^2, \quad 0 = \Delta u + A - \frac{wv^2}{\varepsilon^2} \quad (2.5)$$

with Neumann boundary conditions on Ω . We assume that Ω is a unit disk with the spike located at the center. Near the core of the spike, we rescale:

$$v(x) = V(y), \quad u(x) = U(y) \quad , y = \varepsilon^{-1}x \quad (2.6)$$

Then (2.5) becomes

$$\Delta_y V - V + UV^2 = 0, \quad \Delta_y U + A\varepsilon^2 - UV^2 = 0, \quad y \in \mathbb{R}^2.$$

where Δ_y denotes the Laplacian in y . We expand

$$U = U_0 + \varepsilon^2 U_1 + \dots, \quad V = V_0 + \varepsilon^2 V_1 + \dots.$$

To leading order, we look for a radially symmetric solution given by $V_0 = V_0(\rho)$ and $U_0 = U_0(\rho)$, with $\rho = |y|$. It satisfies the following coupled nonlinear radially symmetric ‘‘core problem’’,

$$\Delta_\rho V_0 - V_0 + U_0 V_0^2 = 0, \quad \Delta_\rho U_0 - U_0 V_0^2 = 0, \quad 0 < \rho < \infty \quad (2.7a)$$

$$V_0 \rightarrow 0, \quad U_0 \sim S \log \rho + \chi(S) \quad \text{as } \rho \rightarrow \infty. \quad (2.7b)$$

The core problem (2.7), was first identified in one dimension in [5]. It is closely related to the phenomenon of self-replicating spots [10, 13, 16].

To determine the source strength S , we integrate the second equation in (2.5) to obtain

$$A\pi = \int_\Omega \frac{uv^2}{\varepsilon^2} dx \sim \int_{\mathbb{R}^2} U_0 V_0^2 dy.$$

On the other hand integrating the second equation in (2.7a) and using the divergence theorem, we obtain

$$2\pi S = \int_{\mathbb{R}^2} U_0 V_0^2 dy$$

so that

$$S = \frac{A}{2}. \quad (2.8)$$

In general, the solution to (2.7a) as well as the function $\chi(S)$ in (2.7b) must be computed numerically. This was done for example in [10, 13, 16]. Figure 2(b) shows the function $\chi(S)$. However for small S , equations (2.7a) become weakly coupled since U_0 becomes nearly constant and we may estimate the solution to (2.7a) as follows. Assume that $S \ll 1$ and $U_0(y) \sim U_0$ is constant to leading order in S . Then V_0, U_0 satisfy at leading order,

$$V_0(y) = w(y)\sigma; \quad U_0(y) = 1/\sigma \quad (2.9)$$

where w is the unique positive ground-state solution to

$$\Delta w - w + w^2 = 0; \quad w \rightarrow 0 \text{ as } |y| \rightarrow \infty; \quad (2.10)$$

and

$$2\pi S \sim \sigma \int w^2 dy; \quad \chi(S) \sim \frac{1}{\sigma}.$$

This yields an asymptotic expression

$$A \sim 2\sigma \int_0^\infty w^2(\rho)\rho d\rho, \quad S \sim \sigma \int_0^\infty w^2(\rho)\rho d\rho, \quad \chi(S) \sim \frac{1}{\sigma}. \quad (2.11)$$

The resulting integral is evaluated numerically (see Appendix B). We summarize this construction as follows.

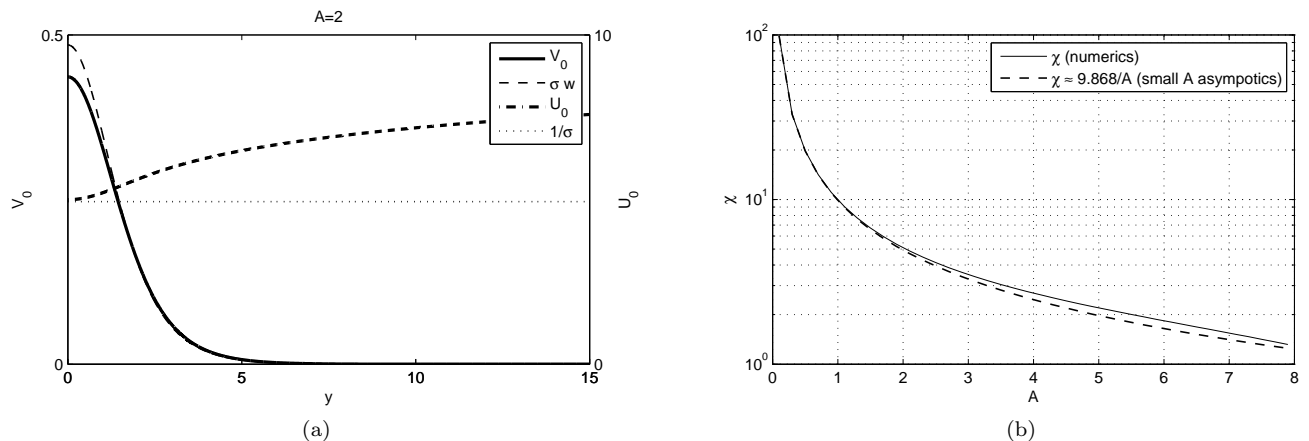


FIG. 3. (a) Core problem V_0, U_0 and its asymptotics (Proposition 2.1). Good comparison between numerics and asymptotics (2.9) is observed even for relatively “large” $A = 2$. (b) A versus χ . Asymptotics denote the regime $A \ll O(1)$ given by $\chi \approx 9.868/A$.

Proposition 2.1 *In the limit $0 < \varepsilon \ll 1$, the leading order steady-state solution to (2.5) near the origin satisfies*

$$v(x) \sim V_0(y), \quad u(x) \sim U_0(y) \quad , y = \varepsilon^{-1}x \quad (2.12)$$

where V_0, U_0 satisfy core problem (2.7) and where the constant S is given by (2.8). In the regime $0 < A \ll O(1)$, we have the asymptotics

$$V_0(x) \sim \sigma w(y), \quad y = \varepsilon x \quad (2.13a)$$

$$U_0(x) \sim \frac{1}{\sigma} \quad (2.13b)$$

where $w(y)$ is the unique ground state given by (2.10) and where

$$\sigma = \frac{1}{2 \int_0^\infty w^2 \rho d\rho} A \approx \frac{A}{9.868} \ll 1. \quad (2.13c)$$

Figure 2(b) shows the graph of S versus $\chi(S)$, as well as its asymptotic approximation. While the asymptotics are formally valid in the regime $A \ll 1$, they agree well with full numerics even when A is relatively large. For example when $A = 2$, full numerics yield $\chi \approx 5.103$ whereas formula (2.11) yields $\sigma \approx 0.2026$, $\chi \approx 4.934$, for a relative error of only 3%. Note also that this error is independent of ε to leading order. Figure 2(a) gives a comparison between $V_0(x)$ and $\sigma w(y)$ with $A = 2$. Excellent agreement is observed. This is in part because the effective small parameter is $\sigma \approx 0.2 \ll 1$ when $A = 2$.

3. STABILITY: LARGE (MODE ZERO) EIGNEVALUE

Having constructed the steady state, we now consider its stability. Linearizing around the steady state in (1.1) we write.

$$u(x, t) = v(r) + e^{\lambda t} \phi(x), \quad u(x, t) = u(r) + e^{\lambda t} \psi(x)$$

The linearized system of (1.1) then becomes:

$$\begin{cases} \lambda \phi = \varepsilon^2 \Delta \phi - \phi + v^2 \psi + 2uv\phi & x \in \Omega \\ \tau \lambda \psi = \Delta \psi - \frac{1}{\varepsilon^2} (v^2 \psi + 2uv\phi) & x \in \Omega \\ \partial_n \phi = 0 = \partial_n \psi & x \in \partial\Omega \end{cases} \quad (3.14)$$

In the inner region, we expand

$$\phi = e^{im\theta} (\Phi_0(\rho) + \varepsilon^2 \Phi_1(\rho) + \dots) \quad \psi = e^{im\theta} (\Psi_0(\rho) + \varepsilon^2 \Psi_1(\rho) + \dots) \quad \rho = |y| \quad y = \varepsilon^{-1}x \quad (3.15)$$

where $y = \rho(\cos \theta, \sin \theta)$. Substituting (3.15) into (3.14), then to leading order we obtain the following radially symmetric eigenvalue problem:

$$\begin{aligned}\lambda\Phi_0 &= \Delta_m\Phi_0 - \Phi_0 + V_0^2\Psi_0 + 2U_0V_0\Phi_0 \\ 0 &= \Delta_m\Psi_0 - (V_0^2\Psi_0 + 2U_0V_0\Phi_0)\end{aligned}\tag{3.16}$$

Here $\Delta_m\Phi_0 \equiv \partial_{\rho\rho}\Phi_0 + \rho^{-1}\partial_\rho\Phi_0 - m^2\rho^{-2}\Phi_0$. and U_0, V_0 are solutions to (2.7).

Because of the decay term in the equation for Φ_0 , we assume that Φ_0 decays exponentially for large $|y|$. On the other hand, the appropriate far-field boundary condition for Ψ_0 depends on whether $m = 0$ or $m \geq 1$.

We begin by considering the mode $m = 0$. In this case the far-field conditions for Ψ_0 exhibits logarithmic growth, $\Psi_0 \sim C \log |y| + B$, $|y| \gg 1$. We can scale the eigenfunction to set $C = 1$, so that Ψ_0 then satisfies

$$\Psi_0 \sim \ln |y| + B, \quad |y| \gg 1.\tag{3.17}$$

By integrating over the equation for Ψ_0 and using the Divergence theorem, this scaling is equivalent to

$$\int_{\mathbb{R}^2} (V_0^2\Psi_0 + 2U_0V_0\Phi_0) = 2\pi.\tag{3.18}$$

The constant B is determined by matching to the outer region. Since v is assumed to decay away from the spike, using (3.18) we have

$$\int_{\Omega} \frac{1}{\varepsilon^2} (v^2\psi + 2uv\phi) dx \sim 2\pi$$

and the outer problem for ψ is

$$\lambda\tau\psi = \Delta\psi - 2\pi\delta(x) \text{ inside } \Omega; \quad \partial_n\psi = 0 \text{ on } \partial\Omega\tag{3.19}$$

whose solution is given by

$$\psi(x) \sim \frac{K'_0(\sqrt{\tau\lambda})}{I'_0(\sqrt{\tau\lambda})} I_0(\sqrt{\tau\lambda}r) - K_0(\sqrt{\tau\lambda}r), \quad r = |x|.\tag{3.20}$$

Expanding for small r we have

$$\begin{aligned}\psi(x) &\sim \log(r) + \frac{K'_0(\sqrt{\tau\lambda})}{I'_0(\sqrt{\tau\lambda})} - \log(2) + \gamma + \log(\sqrt{\lambda\tau}) \quad \text{as } r \rightarrow 0 \\ &\sim \log(|y|) + \frac{K'_0(\sqrt{\tau\lambda})}{I'_0(\sqrt{\tau\lambda})} + \log\left(\frac{e^\gamma}{2}\sqrt{\varepsilon^2\lambda\tau}\right).\end{aligned}\tag{3.21}$$

Note that the above expansion assumes that $\sqrt{\tau\lambda}\varepsilon \ll 1$. This will be shown to be self-consistent later on. Then matching (3.17) and (3.21), yields

$$B = \frac{K'_0(\sqrt{\tau\lambda})}{I'_0(\sqrt{\tau\lambda})} + \log\left(\frac{e^\gamma}{2}\sqrt{\varepsilon^2\lambda\tau}\right).\tag{3.22}$$

Together with (3.16), this provides a closed-system which determines the eigenvalue λ . We summarize this construction:

Proposition 3.1 *In the limit $\varepsilon \rightarrow 0$, the mode-zero eigenvalue λ of the linearized problem (3.14) is asymptotic to the eigenvalue problem (3.16) with $m = 0$ subject to the outer condition (3.17) where B is given by (3.22), as long as $\sqrt{\tau\lambda}\varepsilon \ll 1$.*

We now concentrate on the weakly-coupled regime to $A \ll 1$ given by (2.13c). Substitute the steady-state expansion (2.13) into (3.16) to obtain to leading order

$$\begin{aligned}\lambda\Phi_0 &= \Delta_0\Phi_0 - \Phi_0 + 2w\Phi_0 + w^2\sigma^2\Psi_0 \\ 0 &= \Delta_0\Psi_0 - (w^2\sigma^2\Psi_0 + 2w\Phi_0).\end{aligned}\tag{3.23}$$

Rescale $\Phi_0 = \sigma^2 \hat{\Phi}_0$ and drop the hat to obtain

$$\begin{aligned} \lambda \Phi_0 &= \Delta_0 \Phi_0 - \Phi_0 + 2w\Phi_0 + w^2 \Psi_0 \\ 0 &= \Delta_0 \Psi_0 - \sigma^2 (w^2 \Psi_0 + 2w\Phi_0). \end{aligned} \quad (3.24)$$

whereas (3.18) becomes

$$\int_{\mathbb{R}^2} (w^2 \Psi_0 + 2w\Phi_0) dy = 2\pi\sigma^{-2}. \quad (3.25)$$

In addition, we will assume à-priori that $|\tau\lambda| \gg 1$ (this self-consistency of this assumption will be verified at the end). Under this assumption, using the large-argument expansion of the Bessel functions, the term $\frac{K'_0(\sqrt{\tau\lambda})}{I'_0(\sqrt{\tau\lambda})}$ is exponentially small so that

$$B \sim \log \left(\frac{e^\gamma}{2} \sqrt{\varepsilon^2 \lambda \tau} \right).$$

Furthermore suppose $B \gg 1$. Then we may estimate Ψ_0 by a constant,

$$\Psi_0 \sim \log \left(\frac{e^\gamma}{2} \sqrt{\varepsilon^2 \lambda \tau} \right).$$

We further rescale $\Phi_0(y) = -\Psi_0 \Phi(y)$ which leads to the reduced problem

$$(L_0 - \lambda)\Phi = w^2; \quad (3.26a)$$

$$-2 \int w\Phi + \int w^2 dx = \frac{2\pi\sigma^{-2}}{\log \left(\frac{e^\gamma}{2} \sqrt{\varepsilon^2 \lambda \tau} \right)}. \quad (3.26b)$$

where the operator L_0 is defined by

$$L_0 \Phi := \Delta_0 \Phi - \Phi + 2w\Phi. \quad (3.27)$$

One of the key properties of the operator L_0 is that

$$L_0 w = w^2$$

as can be readily verified using (2.10). This suggests that we seek a Hopf bifurcation point of (3.26) assuming λ is small. We therefore expand in λ

$$\Phi = w + \lambda \Phi_1, \quad \lambda \ll 1 \quad (3.28)$$

to obtain

$$\Phi_1 = L_0^{-1}(w).$$

Define

$$\tau_0 := \left(\frac{e^\gamma}{2} \right)^{-2} \varepsilon^2 \tau \quad (3.29)$$

and assume that λ is purely imaginary,

$$\lambda = i\lambda_I; \quad \lambda_I \ll 1.$$

Then (3.26) becomes

$$-2\lambda_I i \int w L_0^{-1}(w) dy - \int w^2 dy = \frac{2\pi\sigma^{-2}}{\log(\sqrt{i\lambda_I \tau_0})}. \quad (3.30)$$

Using the identity

$$L_0^{-1}w = w + \frac{1}{2}y \cdot \nabla w = w + \frac{1}{2}\rho w'(\rho)$$

and integrating by parts, we obtain

$$2 \int w L_0^{-1}(w) dy = \int w^2 dy \quad (3.31)$$

so that (3.30) becomes

$$\log\left(\sqrt{i\lambda_I\tau_0}\right) = \frac{-2\pi\sigma^{-2}}{\int w^2 dy} \frac{1}{\lambda_I i + 1} = \frac{2 \int w^2 dy}{A^2\pi} \left(\frac{i\lambda_I - 1}{\lambda_I^2 + 1}\right). \quad (3.32)$$

Equating real and imaginary parts we obtain

$$\begin{cases} \frac{1}{2} \log(\lambda_I\tau_0) = \frac{2 \int w^2 dy}{A^2\pi} \frac{-1}{\lambda_I^2 + 1} \\ \frac{\pi}{4} = \frac{2 \int w^2 dy}{A^2\pi} \frac{\lambda_I}{\lambda_I^2 + 1} \end{cases} \quad (3.33)$$

These equations yields, to leading order in $A \ll 1$,

$$\begin{cases} \lambda_I \sim \frac{\pi^2 A^2}{8 \int w^2 dy} \\ \tau_0 = \exp\left(\frac{-4 \int w^2 dy}{A^2\pi}\right) \frac{8 \int w^2 dy}{\pi^2 A^2} \end{cases}, \quad A \ll 1 \quad (3.34)$$

Using (3.29) we finally obtain the critical value of $\tau = \tau_h$ at the Hopf bifurcation point for large eigenvalue:

$$\tau_h = \frac{1}{A^2\varepsilon^2} \exp\left(\frac{-4 \int w^2 dy}{A^2\pi}\right) \frac{2e^{2\gamma} \int w^2 dy}{\pi^2}.$$

We made three assumptions in this derivation: (i) $\lambda\tau \gg 1$; (ii) $\varepsilon^2\tau\lambda \ll 1$ and (iii) $\lambda \ll 1$. Assumptions (ii) and (iii) are satisfied since $A \ll 1$ (see (3.34), (3.29)). On the other hand, assumption (i) is equivalent to $\exp\left(\frac{-4 \int w^2 dy}{A^2\pi}\right) \gg \varepsilon^2$, or $A^2 \gg O\left(\frac{1}{\log \varepsilon^{-1}}\right)$. In summary, we have:

Proposition 3.2 *Suppose that*

$$\frac{1}{\log 1/\varepsilon} \ll A^2 \ll 1.$$

Then the spike solution from Proposition 2.1 undergoes a Hopf bifurcation as τ is increased past $\tau = \tau_{h,large}$ where

$$\tau_{h,large} \sim \frac{1}{A^2\varepsilon^2} a_0 \exp\left(\frac{-a_1}{A^2}\right) \quad (3.35)$$

and

$$a_0 = \frac{4e^{2\gamma} \int_0^\infty w^2(\rho)\rho d\rho}{\pi} \approx 19.929, \quad a_1 = 8 \int_0^\infty w^2(\rho)\rho d\rho \approx 39.474.$$

4. SMALL EIGENVALUES

We study the Hopf bifurcation in the small eigenvalue problem corresponding to the mode $m = 1$ in (3.16). A posteriori analysis reveals that the relevant scaling is

$$\lambda = \lambda_0\varepsilon^2 \quad \tau = \tau_0\varepsilon^{-2}$$

where λ_0 and τ_0 are $O(1)$ with respect to ε . The leading order eigenvalue problem is

$$0 = \Phi_0'' + \frac{1}{\rho}\Phi_0' - \frac{1}{\rho^2}\Phi_0 - \Phi_0 + V_0^2\Psi_0 + 2U_0V_0\Phi_0 \quad (4.36a)$$

$$0 = \Psi_0'' + \frac{1}{\rho}\Psi_0' - \frac{1}{\rho^2}\Psi_0 - (V_0^2\Psi_0 + 2U_0V_0\Phi_0) \quad (4.36b)$$

where $\rho = |y| = |x|/\varepsilon$. The solution to (4.36) is given by:

$$\Phi_0 = \frac{C}{S}V_{0\rho} \quad \Psi_0 = \frac{C}{S}U_{0\rho}. \quad (4.37)$$

and satisfies the far field condition given by

$$\Phi_0 \rightarrow 0, \quad \Psi_0 \sim \frac{C}{\rho}, \quad \text{as } \rho \rightarrow \infty. \quad (4.38)$$

The constant C will be obtained through matching to the outer solution. The outer problem for ψ is

$$\tau_0\lambda\psi = \Delta\psi, \quad r \neq 0$$

subject to $\frac{\partial\psi}{\partial r}(1) = 0$ and $\psi \sim \frac{C\varepsilon e^{i\theta}}{r}$ as $r \rightarrow 0$. This yields an explicit solution

$$\psi = C\varepsilon\sqrt{\tau_0\lambda_0} \left(-\frac{K_1'(\sqrt{\tau_0\lambda_0})}{I_1'(\sqrt{\tau_0\lambda_0})}I_1(\sqrt{\tau_0\lambda_0}r) + K_1(\sqrt{\tau_0\lambda_0}r) \right) e^{i\theta}. \quad (4.39)$$

Recall the small-argument expansion for K_1 and I_1 is given by

$$K_1(z) \sim \frac{1}{z} + \frac{1}{2}z(\log z + b_0) + O(z^2 \ln z), \quad \text{where } b_0 = \gamma - \frac{1}{2} - \ln 2. \quad (4.40a)$$

$$I_1(z) \sim \frac{1}{2}z + O(z^3) \quad (4.40b)$$

Writing (4.39) in inner variables $r = \rho\varepsilon$ and using expansions (4.40) we then obtain

$$\begin{aligned} \psi &\sim \left(\frac{C}{\rho} + \varepsilon^2 \frac{1}{2}C\tau_0\lambda_0\rho \left\{ \log(\sqrt{\tau_0\lambda_0}\rho\varepsilon) - \frac{K_1'(\sqrt{\tau_0\lambda_0})}{I_1'(\sqrt{\tau_0\lambda_0})} + b_0 \right\} \right) e^{i\theta} \\ &\sim e^{i\theta} (\Psi_0(\rho) + \varepsilon\Psi_1(\rho)) \end{aligned}$$

The $O(1)$ terms yields the far-field behaviour for $\Psi(\rho)$ given by (4.38). The $O(\varepsilon^2)$ terms yield the far-field behaviour for $\Psi_1(\rho)$,

$$\Psi_1 \sim \frac{1}{2}C\tau_0\lambda_0\rho \left\{ \log \rho + \log(\sqrt{\tau_0\lambda_0}\varepsilon) - \frac{K_1'(\sqrt{\tau_0\lambda_0})}{I_1'(\sqrt{\tau_0\lambda_0})} + b_0 \right\}, \quad \rho \gg 1. \quad (4.41)$$

To determine λ_0 requires an expansion at the next order. The steady state satisfies

$$\Delta V_1 - V_1 + 2U_0V_0V_1 + U_1V_0^2 = 0, \quad (4.42a)$$

$$\Delta U_1 + A - U_1V_0^2 - 2U_0V_0V_1 = 0, \quad (4.42b)$$

and the corresponding eigenvalue problem is

$$\lambda_0\Phi_0 = \Delta_1\Phi_1 - \Phi_1 + V_0^2\Psi_1 + 2U_0V_0\Phi_1 + 2(V_0U_1 + U_0V_1)\Phi_0 + 2V_0V_1\Psi_0 \quad (4.43a)$$

$$\tau_0\lambda_0\Psi_0 = \Delta_1\Psi_1 - (V_0^2\Psi_1 + 2U_0V_0\Phi_1) - 2(V_0U_1 + U_0V_1)\Phi_0 - 2V_0V_1\Psi_0 \quad (4.43b)$$

subject to the far field condition (4.41).

We express (4.43) in matrix form as

$$\Delta_1\mathbf{W} + M\mathbf{W} = E\mathbf{f}_1 + \mathbf{f}_2, \quad 0 < \rho < \infty \quad (4.44a)$$

$$\mathbf{W} \sim \begin{pmatrix} 0, \\ C_1\rho \ln|\rho| + C_2\rho \end{pmatrix}, \quad \text{as } \rho \rightarrow \infty \quad (4.44b)$$

where:

$$M = \begin{pmatrix} -1 + 2U_0V_0 & V_0^2 \\ -2U_0V_0 & -V_0^2 \end{pmatrix}, \quad E = \begin{pmatrix} -2(U_0V_1 + U_1V_0) & -2V_0V_1 \\ 2(U_0V_1 + U_1V_0) & 2V_0V_1 \end{pmatrix}, \quad (4.44c)$$

$$\mathbf{W} = \begin{pmatrix} \Phi_1 \\ \Psi_1 \end{pmatrix}, \mathbf{f}_1 = \begin{pmatrix} \Phi_0 \\ \Psi_0 \end{pmatrix}, \quad \mathbf{f}_2 = \begin{pmatrix} \lambda_0\Phi_0 \\ \tau_0\lambda_0\Psi_0 \end{pmatrix}, \quad (4.44d)$$

$$C_1 = \frac{1}{2}C\tau_0\lambda_0, \quad C_2 = \frac{1}{2}C\tau_0\lambda_0 \left\{ \log\left(\sqrt{\tau_0\lambda_0\varepsilon}\right) - \frac{K_1'(\sqrt{\tau_0\lambda_0})}{I_1'(\sqrt{\tau_0\lambda_0})} + b_0 \right\}. \quad (4.44e)$$

Let \mathbf{P} be the solution of the adjoint problem,

$$\Delta_1\mathbf{P} + M^t\mathbf{P} = 0 \quad (4.45a)$$

subjected to the far-field behaviour condition

$$\mathbf{P} \sim \begin{pmatrix} 0 \\ \frac{1}{\rho} \end{pmatrix} \quad \text{for } \rho \gg 1. \quad (4.45b)$$

We multiply (4.44a) by $\rho\mathbf{P}^t$ and integrate to obtain

$$\int_0^R \mathbf{P}^t (\Delta_1\mathbf{W} + M \cdot \mathbf{W}) \rho d\rho = \int_0^R \mathbf{P}^t \cdot (E\mathbf{f}_1 + \mathbf{f}_2) \rho d\rho. \quad (4.46)$$

Here, R is a big number which we will take to infinity later. Integrating by parts, the left hand side becomes

$$\int_0^R \mathbf{P}^t (\Delta_1\mathbf{W} + M \cdot \mathbf{W}) \rho d\rho = \left(\mathbf{P}^t \cdot \left(\rho \frac{\partial \mathbf{W}}{\partial \rho} \right) - \left(\rho \frac{\partial \mathbf{P}^t}{\partial \rho} \right) \cdot \mathbf{W} \right)_{\rho=R} \quad (4.47)$$

$$= (2C_1 \ln R + 2C_2 + C_1) \quad (4.48)$$

To calculate the right hand side of (4.46), we introduce $\mathbf{N} = \left(\frac{\partial V_1}{\partial \rho}, \frac{\partial U_1}{\partial \rho} \right)^t$. Upon differentiating the system for V_1 and U_1 with respect to ρ , we obtain

$$\Delta_1\mathbf{N} + M \cdot \mathbf{N} = \begin{pmatrix} -2(U_0V_0)_\rho V_1 - (V_0^2)_\rho U_1 \\ 2(U_0V_0)_\rho V_1 + (V_0^2)_\rho U_1 \end{pmatrix}.$$

The key observation is that

$$E\mathbf{f}_1 = \frac{C}{S} \begin{pmatrix} -2(U_0V_0)_\rho V_1 - (V_0^2)_\rho U_1 \\ 2(U_0V_0)_\rho V_1 + (V_0^2)_\rho U_1 \end{pmatrix} = \frac{C}{S} (\Delta_1\mathbf{N} + M \cdot \mathbf{N})$$

It follows that

$$\begin{aligned} \int_0^R \mathbf{P}^t \cdot (E \cdot \mathbf{f}_1) \rho d\rho &= \frac{C}{S} \int_0^R \mathbf{P}^t \cdot (\Delta_1\mathbf{N} + M \cdot \mathbf{N}) \rho d\rho \\ &= \frac{C}{S} \left(\mathbf{P}^t \cdot \left(\rho \frac{\partial \mathbf{N}}{\partial \rho} \right) - \left(\rho \frac{\partial \mathbf{P}^t}{\partial \rho} \right) \cdot \mathbf{N} \right) \Big|_{\rho=R} \\ &= -2C. \end{aligned}$$

Next we simplify

$$\int_0^R \mathbf{P}^t \cdot \mathbf{f}_2 \rho d\rho = \int_0^R (P_1\Phi_0 + \tau_0 P_2\Psi_0) \lambda_0 \rho d\rho$$

and we further compute

$$\begin{aligned} \int_0^R \tau_0 P_2 \Psi_0 \lambda_0 \rho d\rho &= \frac{C}{S} \tau_0 P_2 U_0 \lambda_0 \rho \Big|_0^R - \frac{C}{S} \int_0^R \tau_0 (P_2 \rho)_\rho U_0 \lambda_0 d\rho \\ &= \frac{C}{S} \tau_0 \lambda_0 (S \log(R) + \chi(S)) - \frac{C}{S} \int_0^R \tau_0 (P_2 \rho)_\rho U_0 \lambda_0 d\rho. \end{aligned}$$

In summary, we obtain that the right hand side of (4.46) simplifies to

$$\int_0^R \mathbf{P}^t \cdot (E\mathbf{f}_1 + \mathbf{f}_2) \rho d\rho = \lambda_0 \int_0^R P_1 \Phi_0 \rho d\rho + C\tau_0 \lambda_0 \log(R) + \frac{C\tau_0 \lambda_0}{S} \chi(S) - \frac{C}{S} \int_0^R \tau_0 (P_2 \rho)_\rho U_0 \lambda_0 d\rho - 2C. \quad (4.49)$$

Equating (4.48) and (4.49), note that the $\log R$ terms cancel each other out and after factoring out C , and we finally obtain

$$\lambda_0 \int_0^R P_1 \frac{1}{S} V_{0\rho} \rho d\rho + \frac{\tau_0 \lambda_0}{S} \chi(S) - \int_0^R \tau_0 (P_2 \rho)_\rho U_0 \lambda_0 d\rho - 2 = \tau_0 \lambda_0 \left(\log \left(\frac{\sqrt{\tau_0 \lambda_0} \varepsilon}{2} \right) - \frac{K'_1(\sqrt{\tau_0 \lambda_0})}{I'_1(\sqrt{\tau_0 \lambda_0})} + \gamma \right)$$

or

$$\frac{\lambda_0 \kappa_1 - \tau_0 \lambda_0 \kappa_2}{S} = \tau_0 \lambda_0 \left(\log \left(\frac{e^\gamma}{2} \sqrt{\tau_0 \lambda_0} \varepsilon \right) - \frac{K'_1(\sqrt{\tau_0 \lambda_0})}{I'_1(\sqrt{\tau_0 \lambda_0})} \right) + 2 \quad (4.50a)$$

where κ_1 and κ_2 are given by

$$\kappa_1 := \int_0^\infty P_1 V_{0\rho} \rho d\rho, \quad \kappa_2 := \int_0^\infty (P_2 \rho)_\rho [U_0 - \chi(S)] d\rho. \quad (4.50b)$$

Next, we seek a Hopf bifurcation for (4.50). Setting $\lambda_0 = i\lambda_I$ in (4.50a) and equating real and imaginary parts yields $\tau_0 \lambda_I = \omega_c$ where ω_c satisfies

$$\omega_c \operatorname{Im} \left(\log(\sqrt{i\omega_c}) - \frac{K'_1(\sqrt{i\omega_c})}{I'_1(\sqrt{i\omega_c})} \right) - 2 = 0 \quad (4.51a)$$

and

$$\tau_0 = \frac{\kappa_1}{S \operatorname{Re} \left(-\frac{K'_1(\sqrt{i\omega_c})}{I'_1(\sqrt{i\omega_c})} + \log \left(\frac{e^\gamma}{2} \sqrt{i\omega_c} \varepsilon \right) \right) + \kappa_2} \quad (4.51b)$$

A remarkable fact is that the equation (4.51a) is independent of any parameters. Numerical plotting shows that there is a unique solution to (4.51a) given by

$$\omega_c \approx 3.02603687. \quad (4.51c)$$

Expression (4.51b) is further simplified by rewriting

$$\operatorname{Re} \left(-\frac{K'_1(\sqrt{i\omega_c})}{I'_1(\sqrt{i\omega_c})} + \log \left(\frac{e^\gamma}{2} \sqrt{i\omega_c} \varepsilon \right) \right) = \alpha_1 + \log(\varepsilon)$$

where

$$\alpha_1 := \operatorname{Re} \left(-\frac{K'_1(\sqrt{i\omega_c})}{I'_1(\sqrt{i\omega_c})} \right) + \log \left(\frac{e^\gamma}{2} \sqrt{\omega_c} \right) = -0.14623425. \quad (4.52)$$

In general, the constants κ_1, κ_2 must be computed numerically. However asymptotic expansion is available in the intermediate regime, when A is small, and is given in Appendix A. We summarize.

Proposition 4.1 *The translational eigenvalue corresponding to mode $m = 1$ of the steady state in Proposition 2.1 undergoes a Hopf bifurcation as τ is increased past $\tau \sim \tau_{h,small}$ where*

$$\tau_{h,small} = \frac{1}{\varepsilon^2} \frac{\kappa_1}{\frac{A}{2} (\log \varepsilon + \alpha_1) + \kappa_2}. \quad (4.53)$$

The constants κ_i are independent of ε (depend only on A) and are given in (4.50b). The constant $\alpha_1 = -0.1462342$ is a universal constant defined through (4.52). In the asymptotic limit $A \ll 1$, the formula (4.53) simplifies to

$$\tau_{h,small} = \frac{1}{\varepsilon^2 A^2} \frac{2\kappa_{10}}{\log \frac{1}{\varepsilon} - \alpha_1 - 2\kappa_{20}}. \quad (4.54)$$

where

$$\kappa_{10} \approx 9.86855; \quad \kappa_{20} \approx 0.1441$$

whose exact value is derived in Appendix A.

Figure 2 shows a very good agreement between the full numerical simulations of the eigenvalue problem (3.14) and formula (4.54).

5. THRESHOLD CROSSING

As Figure 2 shows, the Hopf curves $\tau_{h,large}$ and $\tau_{h,small}$ intersect as A is increased at some critical value $A = A_c$. Having computed asymptotically the Hopf bifurcations for both small and large eigenvalues, we are finally in position to determine this crossing by equating $\tau_{h,large} = \tau_{h,small}$ (where $\tau_{h,large}$ and $\tau_{h,small}$ are given in Propositions 3.2 and 4.1, respectively). Solving for A yields

$$A_c \sim \frac{c_1}{\left[\ln\left(c_2 \ln \frac{1}{\varepsilon} + c_3\right)\right]^{1/2}} \quad (5.55)$$

where

$$\begin{aligned} c_1 &= a_1^{1/2} \approx 6.2828; \\ c_2 &= \frac{e^{2\gamma}}{\pi} \approx 1.00975, \\ c_3 &= \frac{(-\alpha_1 - 2\kappa_{20})a_0}{2\kappa_{10}} \approx -0.14334. \end{aligned}$$

From the formulas for $\tau_{h,large}$ and $\tau_{h,small}$, it is clear that if $A < A_c$, the height oscillations are triggered before position oscillations, whereas the opposite is true if $A > A_c$. This is the main result of the paper. We summarize.

Proposition 5.1 *Let A_c as given in (1.3) with $\varepsilon \ll 1$. Suppose that $A < A_c$. Then height oscillations are triggered before the position oscillations as τ is increased just past $\tau_{h,large}$. Suppose that $A > A_c$. Then position oscillations are triggered before height oscillations as τ is increased just past $\tau_{h,small}$.*

Note that the derivation required that $O\left(\frac{1}{\log \frac{1}{\varepsilon}}\right) \ll A^2 \ll O(1)$. Both of these conditions are clearly satisfied in the critical regime $A^2 = O(A_c^2) = O\left(\frac{1}{\log(\log \frac{1}{\varepsilon})}\right)$.

Although in theory, the formula for A_c is valid as $\varepsilon \rightarrow 0$, the log-log scaling has a horrible convergence rate. It is then all the more surprising that the formula (1.3) is able to predict the threshold within a reasonable accuracy, even when $\varepsilon = 0.02$. To further validate this result, we computed A_c numerically up to $\varepsilon = O(10^{-3})$. The result is summarized in the table in Figure 2. Attempting to compute at such small ε values required the use of a non-uniform grid to compute eigenvalues numerically. We then used a numerical root solver and continuation to adjust A until $\tau_{h,large} = \tau_{h,small}$. We validated our computations by doubling the number of meshpoints. The prediction given by (1.3) is increasingly accurate with each halving of ε , although as expected from a log-log scaling, the improvement in accuracy is very slow.

6. ROTATING SPOT

When the spike is destabilized via translational instabilities, it starts to move as illustrated in figure 1, and may eventually settling into a circular orbit, rotating with some frequency ω_0 around some radius r_0 . The goal of this section is to compute ω_0 and r_0 asymptotically. Before proceeding, it is convenient to rescale

$$\tau = \frac{\tau_0}{\varepsilon^2}, \quad s = \varepsilon^2 t,$$

so that the problem (1.1) becomes

$$\varepsilon^2 v_s = \varepsilon^2 \Delta v - v + v^2 u, \quad \tau_0 u_s = \Delta u + A - \frac{v^2 u}{\varepsilon^2}. \quad (6.56)$$

Let $x_0(s)$ be the location of the spot. To make further progress, we make the ansatz that the spot travels along a circle of radius r_0 with constant angular velocity ω_0 , so that both u and v undergo a rigid rotation. That is, we assume

$$x_0(s) = e^{i\omega_0 s} r_0 \quad (6.57)$$

and $u(x, s) = u(xe^{-i\omega_0 s})$, $v(x, s) = v(xe^{-i\omega_0 s})$. We will estimate inner and outer region and perform matching in order to obtain a solvability condition which will determine the radius and the angular velocity of the spot.

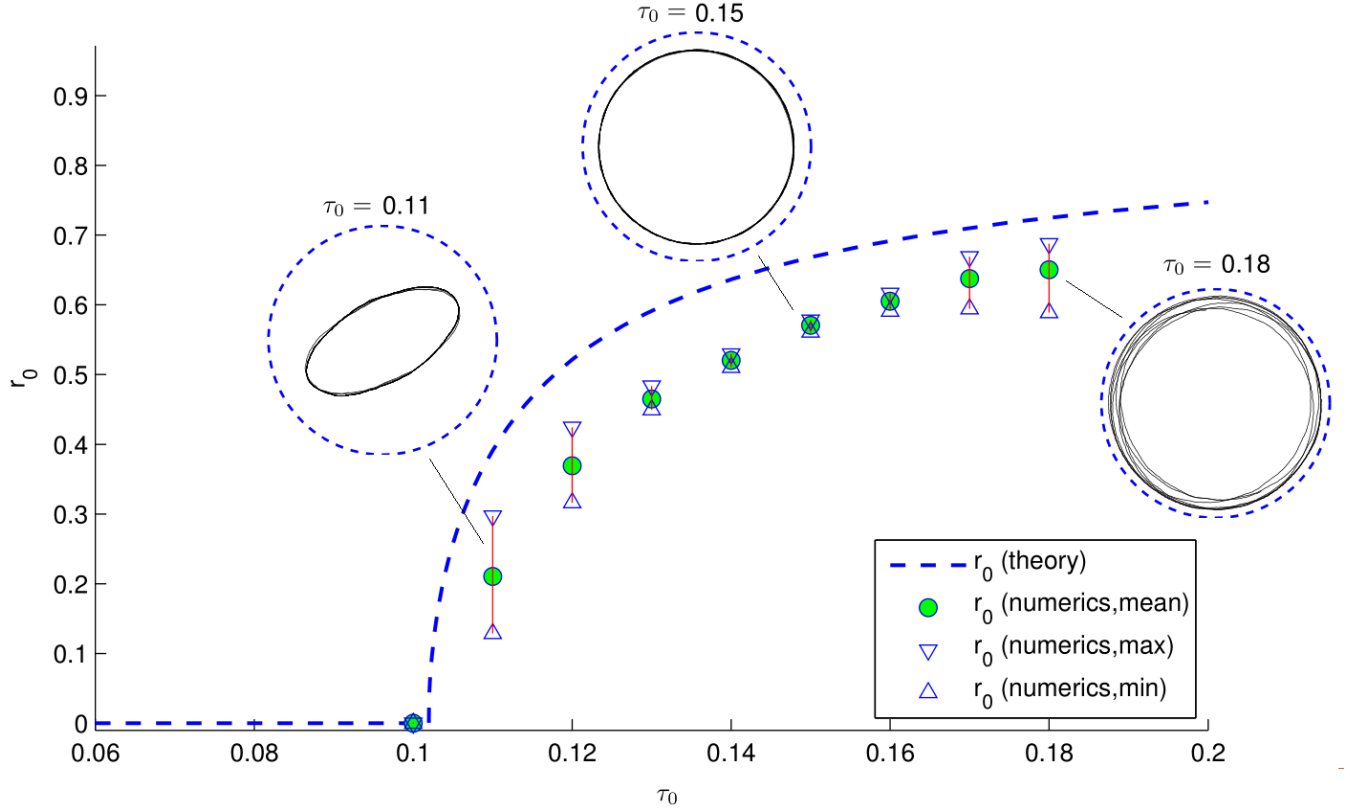


FIG. 4. Radius of rotating spot as a function of $\tau_0 = \tau\varepsilon^2$. Parameter values are $A = 8$ and $\varepsilon = 0.02$. Dashed line is the asymptotic theory given by Proposition 6.1. Circle is the average long-time radius as observed from direct numerical simulations. Inserts show the long-time spike trajectory for τ_0 as indicated (with numerical trajectory shown in solid line and the theoretical rotating-spot trajectory of radius r_0 shown in dashed line).

Outer region. Away from spike location, we estimate the outer problem for u by

$$\Delta u + A = 2\pi S\delta(x - x_0) + \tau_0 u_s \quad (6.58)$$

with Neumann boundary condition $\partial_n u = 0$, $x \in \partial\Omega$. Here, S is defined by

$$2\pi S = \int \frac{uw^2}{\varepsilon^2} dx \sim \int_{\mathbb{R}^2} UV^2 dy, \quad y = \frac{x - x_0(s)}{\varepsilon}$$

The relation between S and A is determined by integrating (6.58) to obtain

$$\pi A = 2\pi S + \tau_0 \frac{d}{ds} \left(\int_{\Omega} u dx \right). \quad (6.59)$$

But since we assumed that u is rigidly rotating, the integral term $\int_{\Omega} u dx$ is independent of time s so that – just as for stationary spot – (6.59) simplifies to

$$S = \frac{A}{2}. \quad (6.60)$$

We write u as

$$u(x, s) = 2SG(x, s) + C$$

where G satisfies

$$\begin{cases} \Delta G + 1 = \pi\delta(x - x_0(s)) + \tau_0 G_s & ; & x_0(s) = e^{i\omega_0 s} r_0, \\ \partial_n G = 0, & x \in \partial\Omega; & \int G dx = 0 \end{cases} \quad (6.61)$$

and C is some (irrelevant for dynamics) constant. We now show that to leading order, (6.61) has the following singularity structure

$$G(x) = \frac{1}{2} \log |x - x_0| + \frac{\tau_0}{4} \dot{x}_0 \cdot (x - x_0) \log |x - x_0| + R_0(x, x_0). \quad (6.62)$$

where R_0 is the ‘‘regular part’’, in the sense that its gradient exists at $x = x_0$; we give explicit expression for R_0 in appendix C. Note that when $\tau_0 = 0$, this corresponds to the usual Modified Green’s function on a disk; however the non-zero τ_0 induces an additional singularity term $\dot{x}_0 \cdot (x - x_0) \log |x - x_0|$. This latter term is ‘‘singular’’ in the sense that its gradient is infinite as $x \rightarrow x_0$ and therefore needs to be ‘‘peeled off’’.

To see where this singularity comes from, first consider the source that moves along y -axis, with some speed c , $x_0(s) = (0, cs)$ on all of space; the free-space moving source Green’s function then satisfies

$$\Delta G = \tau_0 G_s + \pi \delta(x - x_0(s)); \quad x \in \mathbb{R}^2 \text{ and } x_0(s) = (0, cs) \quad (6.63)$$

In this case, transforming into co-moving coordinates $x = (\xi, \eta) + (0, cs)$ yields

$$G_{\xi\xi} + G_{\eta\eta} + c\tau_0 G_\eta = \pi \delta(\xi) \delta(\eta).$$

This problem has an exact solution of the form

$$G(\xi, \eta) = -\frac{1}{2} e^{-\frac{c\tau_0}{2}\eta} K_0\left(\frac{c\tau_0}{2}r\right), \quad r = \sqrt{\xi^2 + \eta^2}. \quad (6.64)$$

We then expand for small r and y using Taylor expansions $K_0(z) \sim -\log z$, $e^{c/2\eta} \sim 1 + \frac{c\tau_0}{2}\eta$ which yields

$$G(\xi, \eta) \sim \frac{1}{2} \left(1 - \frac{c\tau_0}{2}\eta\right) \log r + \dots \quad (6.65)$$

This also explains the choice of the constant $\frac{-1}{2}$ in (6.64) which gives the correct leading order behaviour $G \sim \frac{1}{2} \log r$ independent of $c\tau_0$. Replacing $c\eta$ by $\dot{x}_0 \cdot (x - x_0)$ and r by $|x - x_0|$ indeed yields the singularity structure (6.62). Further expanding x near x_0 , the outer problem for $u(x)$ is then given by

$$u(x) \sim S \log |x - x_0| - \frac{\tau_0 S}{2} \dot{x}_0 \cdot (x - x_0) \log |x - x_0| + 2S(x - x_0) \cdot \nabla R_0 + C, \quad x \rightarrow x_0. \quad (6.66)$$

where $\nabla R_0 = \nabla_x R_0(x, x_0)|_{x=x_0}$ and C is some constant.

Inner region. In the inner region near the spot, we rescale

$$y = \frac{x - x_0(s)}{\varepsilon}; \quad v(x, t) = V(y) \quad u(x, t) = U(y).$$

Then V, U satisfies

$$\begin{cases} -\varepsilon \nabla_y V \frac{dx_0}{ds} = \Delta_y V - V + UV^2 \\ -\tau_0 \varepsilon \nabla_y U \frac{dx_0}{ds} = \Delta_y U + A\varepsilon^2 - UV^2 \end{cases} \quad (6.67)$$

We then expand in ε ,

$$U = U_0 + \varepsilon U_1 + \dots, \quad V = V_0 + \varepsilon V_1 + \dots. \quad (6.68)$$

At the leading order we have

$$\begin{cases} \Delta V_0 - V_0 + U_0 V_0^2 = 0 \\ \Delta U_0 - U_0 V_0^2 = 0 \end{cases}. \quad (6.69)$$

At the next order we obtain

$$\begin{cases} \Delta V_1 - V_1 + 2U_0 V_0 V_1 + V_0^2 U_1 = -\nabla V_0 \cdot \dot{x}_0 \\ \Delta U_1 - 2U_0 V_0 V_1 - V_0^2 U_1 = -\tau_0 \nabla U_0 \cdot \dot{x}_0 \end{cases} \quad (6.70)$$

We assume that V_0, V_1 decays exponentially in the far field $|y| \gg 1$. To obtain the far-field behaviour for U_0 and U_1 , we rewrite the outer expansion (6.66) in the inner variables. This yields

$$u(x) = S \log \varepsilon |y| + \frac{\tau_0 S}{2} \dot{x}_0 \cdot y \varepsilon \log \varepsilon |y| + 2S \nabla R_0 \cdot y \varepsilon + C. \quad (6.71)$$

Upon collecting like terms in ε (while treating $\log \varepsilon$ as an $O(1)$ constant with respect to ε), we obtain

$$U_0 \sim S \log |y| + \chi(S), \quad |y| \gg 1; \quad (6.72)$$

The function $\chi(S)$ is the same as in (2.7) and the constant C in (6.71) determined through the relationship $\chi(S) = S \log \varepsilon + C$.

At the next order we obtain

$$U_1 \sim \frac{\tau_0 S}{2} \dot{x}_0 \cdot y \log |y| + \left(2S \nabla R_0 - \frac{\tau_0 S}{2} \dot{x}_0 \log \varepsilon \right) \cdot y, \quad |y| \gg 1.$$

Following the derivation in §4, we rewrite the system (6.70) as

$$\Delta W + M \cdot W = f, \quad y \in \mathbb{R}^2 \quad (6.73a)$$

$$W \sim (0, -\frac{S\tau_0}{2} \dot{x}_0 \cdot y \ln |y| + \vec{b} \cdot y)^t, \quad \text{as } |y| \rightarrow \infty \quad (6.73b)$$

where

$$\vec{b} = \frac{\tau_0 S}{2} \dot{x}_0 \log \varepsilon + 2S \nabla R_0, \quad (6.73c)$$

$$M = \begin{pmatrix} -1 + 2U_0 V_0 & V_0^2 \\ -2U_0 V_0 & -V_0^2 \end{pmatrix}, \quad \mathbf{W} = \begin{pmatrix} V_1 \\ U_1 \end{pmatrix}, \quad \mathbf{f} = \begin{pmatrix} -\nabla_y V_0 \cdot \dot{x}_0 \\ -\tau_0 \nabla_y U_0 \cdot \dot{x}_0 \end{pmatrix}. \quad (6.73d)$$

As in §4, to formulate the solvability condition, we let $P(\rho) = (P_1(\rho), P_2(\rho))^t$ be the solution to the homogeneous adjoint problem associated with (4.44a), given by (4.45). Define

$$P_c = P(\rho) \cos \theta, \quad P_s = P(\rho) \sin \theta \quad (6.74)$$

where $\cos \theta = \frac{y_1}{|y|}$ and $\sin \theta = \frac{y_2}{|y|}$; note that P_c and P_s both satisfy $\Delta P + M^t P = 0$.

Multiply (6.73a) by P_c^t and integrate by parts over a ball of large radius R to obtain the solvability condition

$$\int_{B_R} P_c^t \cdot f dy = \int_{\partial B_R} P_c^t \cdot \partial_\rho W - W \cdot \partial_\rho P_c^t dy. \quad (6.75)$$

The left hand side of (6.75) simplifies to

$$\int_{B_R} P_c^t \cdot f dy = -\pi \int_0^R (P_1 V_{0\rho} + \tau_0 P_2 U_{0\rho}) \dot{x}_{01} \rho d\rho \quad (6.76)$$

$$\sim -\pi \dot{x}_{01} \pi (\kappa_1 + \tau_0 S \log R - \tau_0 \kappa_2) \quad (6.77)$$

where κ_1, κ_2 are defined in (4.50b).

The right and side of (6.75) simplifies to

$$\int_{\partial B_R} P_c^t \cdot \partial_\rho W - W \cdot \partial_\rho P_c^t dy = \pi \left(-S \tau_0 \dot{x}_{01} \left[\frac{1}{2} + \ln R \right] + 2b_1 \right) \quad (6.78)$$

where b_1 is the first component of vector b in (6.73c). Equating (6.77) and (6.78), note that the $\log R$ terms cancel each other out and we finally obtain

$$-(\kappa_1 - \tau_0 \kappa_2) \dot{x}_{01} = -\frac{S}{2} \tau_0 \dot{x}_{01} + 2b_1.$$

The second solvability condition involving \dot{x}_{01} is obtained similarly by using P_s instead of P_c . The two solvability conditions together yield

$$-(\kappa_1 - \tau_0 \kappa_2) \dot{x}_0 = -\frac{S}{2} \tau_0 \dot{x}_0 + 2 \left(2S \nabla R_0 - \frac{\tau_0 S}{2} \dot{x}_0 \log \varepsilon \right). \quad (6.79)$$

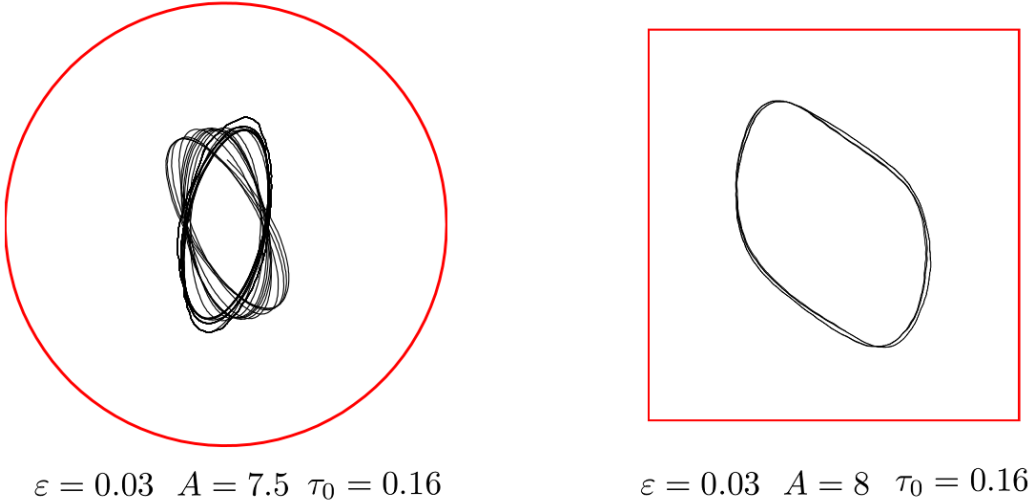


FIG. 5. Complex spot trajectories. Left the domain is a unit disk. Right: the domain is a square of area π .

Solving for \dot{x}_0 and using $S = A/2$ then yields

$$\frac{d}{ds}x_0 = \beta \nabla R_0 \quad \text{where } \beta = \frac{1}{\tau_0 \left(\frac{1}{4} \log \varepsilon + \frac{1}{8} + \frac{\kappa_2}{2A} \right) - \frac{\kappa_1}{2A}} \quad (6.80)$$

In Appendix C we derive an exact expansion for R_0 in terms of an infinite series of Bessel functions. By symmetry, we may assume without loss of generality that x_0 lies on the positive x-axis (i.e. $s = 0$). Then $\frac{d}{ds}x_0|_{s=0} = (0, \omega_0 r_0)$ and we write:

$$\nabla R_0(x, x_0)|_{x_0=(r_0, 0), x=x_0} = (F_1(r_0, \omega), F_2(r_0, \omega)), \quad \text{where } \omega = \omega_0 \tau_0, \quad (6.81)$$

with F_1, F_2 given in (C.7). Equation (6.81) is then equivalent to $F_1 = 0, \omega_0 r_0 = F_2$, or

$$F_1(r_0, \omega) = 0; \quad \tau_0 = \frac{2\kappa_1}{A \left(\log \varepsilon + \frac{1}{2} - \frac{4F_2(r_0, \omega)}{\omega r_0} \right) + \kappa_2}; \quad \omega_0 = \omega / \tau_0. \quad (6.82)$$

In addition, as we show in Appendix C, the threshold $\tau_{h,small}$ of Proposition 4.1 is recovered in the limit $r_0 \rightarrow 0$. We summarize our construction as follows.

Proposition 6.1 *The Schnakenberg model (1.1) on a unit disk admits a rotating spot solution for $\tau > \tau_{h,small}$, where $\tau_{h,small}$ is the Hopf bifurcation value with respect to translational eigenvalues as given in Proposition 4.1. The spot center $x_0 = r_0 e^{i\omega_0 \varepsilon^2 t}$ rotates with angular velocity $\omega_0 \varepsilon^2$ and radius r_0 . as determined through (6.82).*

Figure 4 shows a comparison between the numerical simulations of the full system (1.1) and the asymptotic prediction for the radius of the rotating spot. For example take $\tau_0 = 0.15, A = 8, \varepsilon = 0.02$. Then using (4.50b) we first compute $\kappa_1 = -1.2938$ and $\kappa_2 = 3.54334$ by solving the radial core problem and the adjoint eigenvalue problem using a boundary value problem solver in Matlab (`bvp4c`). From (6.82) we then obtain $r_0 = 0.669$ and $\omega = 6.1994$. Full numerical simulations of the original model (1.1) exhibit a rotating spot whose radius is $r_{0,numeric} \approx 0.57$, in good agreement with the theoretical prediction. Although the Proposition 6.1 applies for any $\tau > \tau_{h,small}$, the rotating spot solution is not always stable as Figure 4 shows. For example when $\tau_0 = 0.11$, the numerical solution appears to be in the shape of an ellipse whereas for $\tau_0 = 0.18$ the radius is close to the theoretical prediction but appears to vary with time, generating an annular region. More complex trajectories are possible as shown in Figure 5.

7. DISCUSSION

We have used formal asymptotics to compute Hopf bifurcation thresholds $\tau = \tau_{h,large}$ and $\tau = \tau_{h,small}$ that induce spike oscillations in either height ($\tau_{h,large}$) or position ($\tau_{h,small}$) for the Schankenberg model. These two thresholds

cross at $A = A_c$. That is, height oscillations dominate ($\tau_{h,large} < \tau_{h,small}$) when $A < A_c$ whereas position oscillations dominate ($\tau_{h,small} < \tau_{h,large}$) when $A > A_c$, where A_c given by (1.3) has an $O(1/\log(\log \varepsilon))$ scaling. Despite the extremely slow decay of A_c as $\varepsilon \rightarrow 0$, the asymptotically computed value of A_c agrees surprisingly well with numerics even with $\varepsilon = 0.01$ (the constants in (1.3) are very important to get a good agreement). We remark that in one dimension, a similar ‘‘double-hopf’’ point was found in several papers [7–9]. However it has an *algebraic* scaling $A_c = O(\varepsilon^{1/6})$ ([8]).

In the regime $\tau_{h,small} < \tau < \tau_{h,large}$, we have constructed a periodic spike solution consisting of a rotating spot inside a unit disk, and computed the radius and speed of the rotation by expanding the underlying Green’s function in terms of complex Bessel series. Numerical experiments suggest that the rotating solution is not always stable – see Figure 4. In particular, for τ just slightly above the bifurcation point $\tau_{h,small}$, the spike trajectory is an ellipse, whereas for τ sufficiently large, the spot path fills out an annulus. It would be a very interesting to study the stability of these rotating spots.

It would be interesting to study more general spot motion and for more general domains. Figure 5 gives some idea of possible trajectories. A preliminary goal is to derive and numerically simulate the reduced equations of motion. The reduced equations of motion comprise a coupled PDE-ODE system with a moving source, analogous to the equations derived in §6. The numerical difficulty is the ODE for the source location requires an extraction of a very weakly singular part of the moving Green’s function.

Circular spot motion is intimately related to the model of a small rotating trap inside an insulated unit disk, which was recently studied in [26, 27]. There, the main goal was to minimize the mean first passage time (MFPT) for a rotating trap $x_0 = r_0 e^{i\omega t}$ (or several rotating traps) as a function of its radius r_0 and its angular velocity ω . It turned out that the optimal radius r_0 and velocity ω have precisely the same relation $F_1(r_0, \omega) = 0$ as we found in Proposition 6.1. As a result, for small angular velocity ($\omega < \omega_c$), it was optimal for the trap to be located at the origin, whereas for $\omega > \omega_c$ it was better for the spot to move. This is the precise analogue of the Hopf bifurcation computed in Proposition 4.1.

Spot motion was also observed for a three-component gas-discharge system [28]. There, the authors also analysed complex spot dynamics, including spot collision and splitting. The initial instability inducing spot motion in this system was further analysed in detail in [29] where theoretical and numerical study of the bifurcation from a stationary to a moving spot was performed. Let us also mention the work [30] where complex motion of a self-propelled deformable particle was studied.

While in many aspects, GM, GS and Schakengerg models are very similar mathematically, the oscillations of spot positions have never been observed in GM model. It would be interesting to have a better understanding of the kind of general conditions that are needed to observe position oscillations.

Appendix A: Estimating κ_1, κ_2 for small A .

In this appendix we compute the asymptotic expansion for κ_1, κ_2 given by (4.50b) for small A . In this limit, we recall from (2.9) that $U_0 \sim \chi = \sigma^{-1}$ and $V_0 \sim \sigma w$ where $\sigma = \frac{A}{2 \int_0^\infty \frac{1}{w^2 \rho d\rho}}$. The adjoint problem (4.45) simplifies to

$$(\partial_{\rho\rho} + \rho^{-1}\partial_\rho - \rho^{-2}) P_1 - P_1 + 2wP_1 - 2wP_2 \sim 0, \quad 0 < \rho < \infty, \quad P_1 \sim 0 \text{ as } \rho \rightarrow \infty \quad (\text{A.1a})$$

$$(\partial_{\rho\rho} + \rho^{-1}\partial_\rho - \rho^{-2}) P_2 + \sigma^2 w^2 (P_1 - P_2) \sim 0, \quad 0 < \rho < \infty, \quad P_2 \sim \rho^{-1}, \text{ as } \rho \rightarrow \infty. \quad (\text{A.1b})$$

The solution to this limiting system is given by

$$P_1 = \sigma^{-2} \left(-\frac{3w_\rho}{\int_0^\infty w^3 s ds} + O(\sigma^2) \right), \quad P_2 = \frac{1}{\rho} \frac{\int_0^\rho w^3 s ds}{\int_0^\infty w^3 s ds} + O(\sigma^2) \quad (\text{A.2})$$

and we then obtain

$$\kappa_1 \sim \frac{-3 \int_0^\infty w_\rho^2 \rho d\rho}{\int_0^\infty w^3 \rho d\rho} \sigma^{-1}, \quad \kappa_2 \sim \frac{1}{\int_0^\infty w^3 \rho d\rho} \int_0^\infty [U_0 - \sigma^{-1}] w^3 \rho d\rho. \quad (\text{A.3})$$

To compute κ_2 further, we let $U_0 - \sigma^{-1} = \sigma \hat{U} + O(\sigma^2)$ where \hat{U} satisfies

$$\Delta \hat{U} = w^2$$

subject to the far-field condition $\hat{U} \sim S \log \rho + 0$, $\rho \gg 1$. The solution to \hat{U} is given by

$$\hat{U}(\rho) = \int_0^\rho \frac{F(s)}{s} ds - \int_1^\infty \frac{F(s) - F(\infty)}{s} ds - \int_0^1 \frac{F(s)}{s} ds$$

where

$$F(s) = \int_0^s w^2(\rho)\rho d\rho;$$

κ_2 is then given by

$$\kappa_2 \sim \sigma \frac{\int_0^\infty \hat{U} w^3 \rho d\rho}{\int_0^\infty w^3 \rho d\rho}.$$

The integrals $\int_0^\infty \hat{U} w^3 \rho d\rho$ is computed numerically. In summary, we obtain the following expansions for κ_1, κ_2 :

$$\kappa_1 \sim -\frac{1}{A}\kappa_{10}; \quad \kappa_2 \sim A\kappa_{20}$$

where (using (B.4)),

$$\kappa_{10} = 2 \int_0^\infty w^2 \rho d\rho; \quad \kappa_{20} = \frac{\int_0^\infty \hat{U} w^3 \rho d\rho}{2 \int_0^\infty w^2 \rho d\rho \int_0^\infty w^3 \rho d\rho}.$$

The numerical estimates for κ_1 and κ_2 , computed using numerical quadrature, are

$$\kappa_{10} \approx 9.8686; \quad \kappa_{20} \approx 0.1441.$$

Appendix B: Some properties of function w

We start from the ground state $w(y) = w(\rho)$, $\rho = |y|$. It satisfies

$$w'' + \frac{w'}{\rho} - w + w^2 = 0, \quad w'(0) = 0, \quad w \rightarrow 0 \quad \text{as } \rho \rightarrow \infty \quad (\text{B.1})$$

Multiplying (B.1) by $w\rho$ and $w'\rho^2$ respectively and integrating over the domain yields

$$-\int_0^\infty w_\rho^2 \rho d\rho - \int_0^\infty w^2 \rho d\rho + \int_0^\infty w^3 \rho d\rho = 0 \quad (\text{B.2})$$

$$\int_0^\infty w^2 \rho d\rho - \frac{2}{3} \int_0^\infty w^3 \rho d\rho = 0 \quad (\text{B.3})$$

Combining these two equations leads to

$$\frac{\int_0^\infty w_\rho^2 \rho d\rho}{\int_0^\infty w^3 \rho d\rho} = \frac{1}{3}, \quad \frac{\int_0^\infty w^2 \rho d\rho}{\int_0^\infty w^3 \rho d\rho} = \frac{2}{3}. \quad (\text{B.4})$$

Finally, we will use the following numerical estimate:

$$\int_0^\infty w^2 \rho d\rho \approx 4.9343$$

It is obtained by solving (B.1) using Matlab's boundary value problem solver `bvp4c`, then using numerical quadrature for the resulting integral.

Appendix C: Green's function for rotating spot

In this appendix we compute explicitly gradient of the regular part of the rotating Green's function, defined through (6.61), (6.62). In the rotating frame, the Green's function G from (6.61) satisfies

$$\frac{\partial^2 G}{\partial r^2} + \frac{1}{r} \frac{\partial G}{\partial r} + \frac{1}{r^2} \frac{\partial^2 G}{\partial \theta^2} + \omega \frac{\partial G}{\partial \theta} = 1 - \pi \delta(r - r_0) \delta(\theta) \quad (\text{C.1})$$

$$\partial_r G = 0 \quad \mathbf{x} \in \partial\Omega. \quad (\text{C.2})$$

where

$$\omega = \tau_0 \omega_0. \quad (\text{C.3})$$

Using separation of variable, we write $G(r, \theta)$ as

$$G = G_0(r) + \sum_{m=1}^{\infty} (G_m(r)e^{im\theta} + c.c.) \quad (\text{C.4})$$

where c.c refers to the complex conjugate of the term involving the summation. Substituting (C.4) into (C.1) and recalling the Neumann boundary condition, we obtain:

$$\frac{\partial^2 G_0}{\partial r^2} + \frac{1}{r} \frac{\partial G_0}{\partial r} = 1 - \pi \delta(r - r_0) \delta(\theta), \quad G_0 \text{ bounded as } r \rightarrow 0, \quad G'_0(1) = 0 \quad (\text{C.5a})$$

$$\frac{\partial^2 G_m}{\partial r^2} + \frac{1}{r} G_m - \frac{m^2}{r^2} G_m + im\omega G_m = -\pi \delta(r - r_0) \delta(\theta), \quad m > 0, \quad G_m \text{ bounded as } r \rightarrow 0, \quad G'_m(1) = 0 \quad (\text{C.5b})$$

For $m > 0$, the homogeneous solution of (C.5b) may be written as

$$G_m(r, \omega) = a_m I_m(c_m r) + b_m K_m(c_m r); \quad c_m \equiv \sqrt{-i\omega m}$$

where $I_m(r)$ and $K_m(r)$ are m-th order modified Bessel functions of the first and second kind, respectively. Solving (C.5b) separately for $r < r_0$ and $r > r_0$, and applying appropriate continuity and jump conditions at $r = r_0$, we obtain the solution for G_m ,

$$G_m(r) = \begin{cases} \frac{1}{2} \left[-\frac{K'_m(c_m)}{I'_m(c_m)} I_m(c_m r_0) + K_m(c_m r_0) \right] I_m(c_m r), & 0 < r < r_0 \\ \frac{1}{2} \left[-\frac{K'_m(c_m)}{I'_m(c_m)} I_m(c_m r) + K_m(c_m r) \right] I_m(c_m r_0), & r_0 < r < 1 \end{cases}, \quad c_m \equiv \sqrt{-i\omega m}, \quad m \neq 0$$

where $I'_m(c_m)$ and $K'_m(c_m)$ denote the derivatives of I_m and K_m evaluated at c_m , respectively. In a similar way, we find that the solution to (C.5) for $G_0(r)$,

$$G_0(r) = \frac{r^2}{4} + \frac{2r_0^2 - 3}{8} - \begin{cases} \frac{1}{2} \log r_0, & 0 < r < r_0 \\ \frac{1}{2} \log r, & r_0 < r < 1 \end{cases}.$$

Recall that

$$R_0 = G - S_1 - S_2$$

where

$$S_1 := -\frac{1}{2} \log |x - x_0|; \quad S_2 := \frac{1}{4} \tau_0 \frac{\partial x_0}{\partial t} \cdot (x - x_0) \log |x - x_0|. \quad (\text{C.6})$$

To calculate R_0 and its gradient, we first expand the singular parts S_1 and S_2 in terms of their Fourier series, then take the limit $\theta \rightarrow 0, r \rightarrow r_0^-$. We have

$$S_1 := -\frac{1}{2} \log |x - x_0| = -\frac{1}{2} \log(r_M) + \frac{1}{2} \sum_{m \geq 1} \frac{\rho^m}{2m} (e^{im\theta} + e^{-im\theta}), \quad \text{where } r_M = \max(r, r_0), \quad \rho = \frac{\min(r, r_0)}{\max(r, r_0)};$$

$$\frac{1}{4} \tau_0 \frac{\partial x_0}{\partial t} \cdot (x - x_0) = -\frac{\omega r r_0}{8} (ie^{i\theta} - ie^{-i\theta});$$

$$S_2 = \frac{\omega r r_0}{8i} \left[\left(\log(r_M) + \frac{\rho^2}{4} \right) e^{i\theta} - \frac{1}{2} \sum_{m \geq 2} \left(\frac{1}{m-1} \rho^{-1} - \frac{1}{m+1} \rho \right) \rho^m e^{im\theta} \right] + c.c.$$

The function F_1 and F_2 defined through (6.81) are then expressed in terms of polar variables as

$$F_1(r_0, \omega) = \partial_r R_0|_{r=r_0^-, \theta=0}; \quad F_2(r_0, \omega) = \frac{1}{r_0} \partial_\theta R_0|_{r=r_0^-, \theta=0}$$

Differentiating with respect to r and θ and then evaluating at $r = r_0^-$ and $\theta = 0$, we finally obtain the following expressions,

$$F_1(r_0, \omega) = \frac{r_0}{2} + \sum_{m \geq 1} \left(2 \operatorname{Re} (G'_m(r_0^-)) - \frac{1}{2r_0} \right) \quad (\text{C.7a})$$

$$r_0 F_2(r_0, \omega) = -\frac{\omega r_0^2}{4} \left[\left(\log(r_0) + \frac{1}{4} \right) \right] - 2 \operatorname{Im} (G_1(r_0^-)) + \sum_{m \geq 2} \left(-2m \operatorname{Im} G_m(r_0^-) + \frac{\omega r_0^2}{4} \frac{m}{m^2 - 1} \right) \quad (\text{C.7b})$$

where

$$G_m(r_0^-) = \frac{1}{2} \left[-\frac{K'_m(c_m)}{I'_m(c_m)} I_m(c_m r_0) + K_m(c_m r_0) \right] I_m(c_m r_0); \quad (\text{C.7c})$$

$$G'_m(r_0^-) = \frac{c_m}{2} \left[-\frac{K'_m(c_m)}{I'_m(c_m)} I_m(c_m r_0) + K_m(c_m r_0) \right] I'_m(c_m r_0), \quad c_m \equiv -i\sqrt{i\omega m}. \quad (\text{C.7d})$$

The Hopf bifurcation threshold derived in Proposition 4.1 corresponds to letting $r_0 \rightarrow 0$. To establish the equivalence between the expression for r_0 in Proposition 6.1 and the threshold $\tau_{h,small}$ in Proposition 4.1, we using the small-argument expansions for K_m and I_m to obtain the leading-order expressions,

$$F_1(r, \omega) = \frac{r_0}{2} + 2 \operatorname{Re} (G'_1(r_0^-)) - \frac{1}{2r_0}; \quad r_0 F_2(r_0, \omega) = -2 \operatorname{Im} (G_1(r_0)) - \frac{\omega r_0^2}{4} \left[\left(\log(r_0) + \frac{1}{4} \right) \right]$$

Further simplifying, we obtain

$$F_1(r_0, \omega) \sim \frac{r_0}{4} \left(-\operatorname{Im} \left(\frac{K'_1(\sqrt{-\omega i})}{I'_1(\sqrt{-\omega i})} \right) \omega + 2 - \frac{\pi\omega}{4} \right), \quad r_0 \ll 1$$

$$F_2(r_0, \omega) \sim \frac{1}{4} r_0 \omega \left(-\operatorname{Re} \left(\frac{K'_1(\sqrt{-\omega i})}{I'_1(\sqrt{-\omega i})} \right) + \frac{1}{2} \log(\omega/4) + \gamma - \frac{1}{2} \right), \quad r_0 \ll 1$$

Setting $F_1 = 0$ and letting $r_0 \rightarrow 0$, we obtain $\omega = \omega_c$ is the root of (4.51a). Then setting $F_2 = 0$ and recalling that $\omega = \omega_0 \tau_0$, one recovers Proposition 6.1.

-
- [1] J. Schnakenberg, Simple chemical reaction systems with limit cycle behaviour, *Journal of theoretical biology* 81 (3) (1979) 389–400.
 - [2] Y. Chen, T. Kolokolnikov, J. Tzou, C. Gai, Patterned vegetation, tipping points, and the rate of climate change, *European Journal of Applied Mathematics* 26 (06) (2015) 945–958.
 - [3] D. L. Benson, J. A. Sherratt, P. K. Maini, Diffusion driven instability in an inhomogeneous domain, *Bulletin of mathematical biology* 55 (2) (1993) 365–384.
 - [4] L. Shaw, J. Murray, Analysis of a model for complex skin patterns, *SIAM Journal on Applied Mathematics* 50 (2) (1990) 628–648.
 - [5] J. E. Pearson, Complex patterns in a simple system, *Science* 261 (5118) (1993) 189–192.
 - [6] A. Doelman, R. A. Gardner, T. J. Kaper, A stability index analysis of 1-D patterns of the Gray-Scott model, no. 737, *American Mathematical Soc.*, 2002.
 - [7] A. Doelman, T. J. Kaper, W. Eckhaus, Slowly modulated two-pulse solutions in the gray-scott model i: Asymptotic construction and stability, *SIAM Journal on Applied Mathematics* 61 (3) (2000) 1080–1102.
 - [8] C. Muratov, V. Osipov, Traveling spike autosolitons in the gray-scott model, *Physica D: Nonlinear Phenomena* 155 (1) (2001) 112–131.
 - [9] T. Kolokolnikov, M. J. Ward, J. Wei, The existence and stability of spike equilibria in the one-dimensional gray-scott model: the pulse-splitting regime, *Physica D: Nonlinear Phenomena* 202 (3) (2005) 258–293.
 - [10] C. Muratov, V. Osipov, Spike autosolitons and pattern formation scenarios in the two-dimensional gray-scott model, *The European Physical Journal B-Condensed Matter and Complex Systems* 22 (2) (2001) 213–221.
 - [11] M. J. Ward, J. Wei, The existence and stability of asymmetric spike patterns for the schnakenberg model, *Studies in Applied Mathematics* 109 (3) (2002) 229–264.
 - [12] J. Wei, M. Winter, Stationary multiple spots for reaction-diffusion systems, *Journal of mathematical biology* 57 (1) (2008) 53–89.
 - [13] T. Kolokolnikov, M. J. Ward, J. Wei, Spot self-replication and dynamics for the schnakenburg model in a two-dimensional domain, *Journal of nonlinear science* 19 (1) (2009) 1–56.

- [14] D. Iron, J. Wei, M. Winter, Stability analysis of turing patterns generated by the schnakenberg model, *Journal of mathematical biology* 49 (4) (2004) 358–390.
- [15] Y. Nishiura, D. Ueyama, Spatio-temporal chaos for the gray–scott model, *Physica D: Nonlinear Phenomena* 150 (3) (2001) 137–162.
- [16] W. Chen, M. J. Ward, The stability and dynamics of localized spot patterns in the two-dimensional Gray-Scott model., *SIAM J. Appl. Dynam. Systems*, 2010.
- [17] W. Chen, M. J. Ward, Oscillatory instabilities and dynamics of multi-spike patterns for the one-dimensional gray-scott model, *European Journal of Applied Mathematics* 20 (2009) 187–214.
- [18] J. Tzou, A. Bayliss, B. Matkowsky, V. Volpert, Stationary and slowly moving localised pulses in a singularly perturbed brusselator model, *European Journal of Applied Mathematics* 22 (5) (2011) 423–453.
- [19] D. Iron, M. J. Ward, J. Wei, The stability of spike solutions to the one-dimensional gierer–meinhardt model, *Physica D: Nonlinear Phenomena* 150 (1) (2001) 25–62.
- [20] M. J. Ward, J. Wei, Hopf bifurcations and oscillatory instabilities of spike solutions for the one-dimensional gierer–meinhardt model, *Journal of Nonlinear Science* 13 (2) (2003) 209–264.
- [21] J. Wei, M. Winter, *Mathematical aspects of pattern formation in biological systems*, Vol. 189, Springer Science & Business Media, 2013.
- [22] T. Kolokolnikov, M. J. Ward, J. Wei, The existence and stability of spike equilibria in the one-dimensional gray–scott model: The low feed-rate regime, *Studies in Applied Mathematics* 115 (1) (2005) 21–71.
- [23] I. Barrass, E. J. Crampin, P. K. Maini, Mode transitions in a model reaction–diffusion system driven by domain growth and noise, *Bulletin of mathematical biology* 68 (5) (2006) 981–995.
- [24] E. Gaffney, N. Monk, Gene expression time delays and turing pattern formation systems, *Bulletin of mathematical biology* 68 (1) (2006) 99–130.
- [25] C.-C. Chen, T. Kolokolnikov, Simple pde model of spot replication in any dimension, *SIAM Journal on Mathematical Analysis* 44 (5) (2012) 3564–3593.
- [26] J. C. Tzou, S. Xie, T. Kolokolnikov, First-passage times, mobile traps, and hopf bifurcations, *Physical Review E* 90 (6) (2014) 062138.
- [27] A. Lindsay, J. Tzou, T. Kolokolnikov, Optimization of first passage times by multiple cooperating mobile traps, Submitted, M3AS.
- [28] Y. Nishiura, T. Teramoto, K.-I. Ueda, Scattering of traveling spots in dissipative systems, *Chaos: An Interdisciplinary Journal of Nonlinear Science* 15 (4) (2005) 047509.
- [29] P. Van Heijster, B. Sandstede, Bifurcations to travelling planar spots in a three-component fitzhugh–nagumo system, *Physica D: Nonlinear Phenomena* 275 (2014) 19–34.
- [30] T. Ohta, T. Ohkuma, Deformable self-propelled particles, *Physical review letters* 102 (15) (2009) 154101.